



UNIVERSITY OF LEEDS

This is a repository copy of *Enabling Autonomous Ultrasound-Guided Tumor Ablation During Robotic Surgery*.

White Rose Research Online URL for this paper:

<https://eprints.whiterose.ac.uk/221008/>

Version: Accepted Version

Proceedings Paper:

Marahrens, N., Jones, D., Stevenson, J. et al. (4 more authors) (2024) Enabling Autonomous Ultrasound-Guided Tumor Ablation During Robotic Surgery. In: 2024 10th IEEE RAS/EMBS International Conference for Biomedical Robotics and Biomechatronics (BioRob). 2024 10th IEEE RAS/EMBS International Conference for Biomedical Robotics and Biomechatronics (BioRob), 01-04 Sep 2024, Heidelberg, Germany. IEEE , pp. 1516-1522. ISBN 979-8-3503-8653-0

<https://doi.org/10.1109/biorob60516.2024.10719947>

© 2024 IEEE. Personal use of this material is permitted. Permission from IEEE must be obtained for all other uses, in any current or future media, including reprinting/republishing this material for advertising or promotional purposes, creating new collective works, for resale or redistribution to servers or lists, or reuse of any copyrighted component of this work in other works.

Reuse

Items deposited in White Rose Research Online are protected by copyright, with all rights reserved unless indicated otherwise. They may be downloaded and/or printed for private study, or other acts as permitted by national copyright laws. The publisher or other rights holders may allow further reproduction and re-use of the full text version. This is indicated by the licence information on the White Rose Research Online record for the item.

Takedown

If you consider content in White Rose Research Online to be in breach of UK law, please notify us by emailing eprints@whiterose.ac.uk including the URL of the record and the reason for the withdrawal request.



eprints@whiterose.ac.uk
<https://eprints.whiterose.ac.uk/>

Enabling Autonomous Ultrasound-Guided Tumor Ablation during Robotic Surgery

Nils Marahrens¹, Dominic Jones¹, Jack Stevenson², James McLaughlan¹, Chandra Shekhar Biyani³, Margaret Lucas² and Pietro Valdastrì¹

Abstract— While technologies such as cryo- or radio-frequency ablation allow for less invasive treatment of tumors than resection, they still require needles to reach the target location with the potential risk of spreading tumor tissue around. High Intensity Focused Ultrasound (HIFUS) on the other hand allows for a completely remote and concentrated delivery of energy to a target location without the need for direct access and is particularly well suited to be robotically guided and thus used as part of an autonomous system. While robotic HIFUS devices have been extensively explored for extracorporeal applications, their application into a laparoscopic setting is still widely unexplored. This paper presents an Ultrasound (US) guided workflow and system concept to allow the integration of a pick-up HIFUS system into a surgical robotic setup. Additionally, a novel sensorised water-filled membrane is developed and evaluated, enabling hybrid force position control that allows for minimising interaction forces with the tissue surface while maintaining sufficient acoustic coupling for ablation. Experiments on a phantom with a HIFUS probe dummy demonstrate the effectiveness of the approach in targeting hidden structures.

I. INTRODUCTION

Recent years have seen a trend towards minituarisation of HIFUS probes into minimally invasive devices [4], [5], [6], [7]. In its inception, the minituarisation of HIFUS devices allow a more localised treatment of tumors rather than needing to penetrate the abdominal wall and layers of fat tissue that can further stretch across the target regions and dampen the ultrasonic waves induced [4], while bearing less risk of harming additional tissue and further spread out cancerous cells outside the tumor region compared to other ablation methods such as Cryoablation (CA) [4]. A key difference to extracorporeal devices is that minimally invasive devices do not include imaging a the center of the lens due to size constraints.

*This work was supported by the Royal Society, by the Engineering and Physical Sciences Research Council (EPSRC) under grant number EP/R045291/1, and by the European Research Council (ERC) under the European Unions Horizon 2020 research and innovation program (grant agreement No 818045).

¹Nils Marahrens, Dominic Jones, James McLaughlan and Pietro Valdastrì are with the Institute of Robotics, Autonomous Systems and Sensing (IRASS), School of Electronic and Electrical Engineering, University of Leeds, Leeds LS2 9JT, UK (e.lnma@leeds.ac.uk; d.p.jones@leeds.ac.uk; p.valdastrì@leeds.ac.uk)

²Jack Stevenson and Margaret Lucas are with Centre for Medical and Industrial Ultrasonics (C-MIU), James Watt School of Engineering, University of Glasgow, Glasgow G12 8QQ, UK (j.stevenson.2@research.gla.ac.uk; margaret.lucas@glasgow.ac.uk)

³Shekhar Biyani is with the Department for Urology, James's University Hospital, Leeds Teachings Hospitals NHS Trust, Leeds, UK (c.s.biyani@leeds.ac.uk)

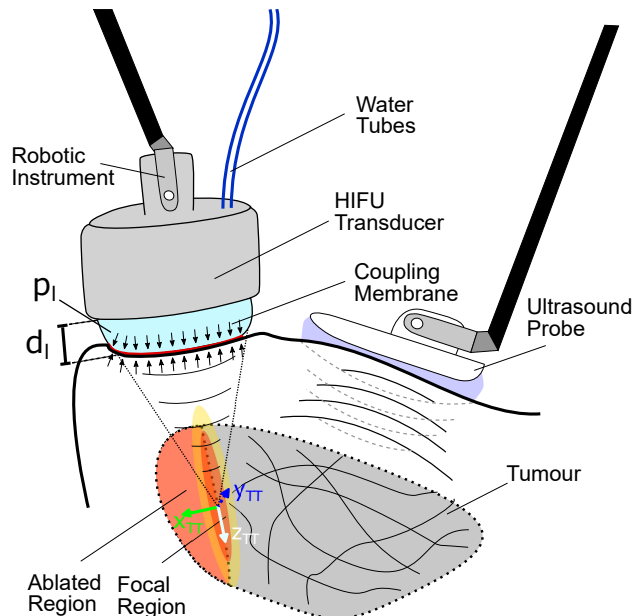


Fig. 1: US-guided HIFUS concept with membrane conforming to surface shape and including the used tool tip frame with z_{TT} being perpendicular to the transducer surface.

While the application of ablation devices in a laparoscopic setting, in particular HIFUS, has been extensively researched [6], [7], [4], this is not the case for robotically guided probes. To the best of our knowledge the only translation onto a robotic system is presented in the extended abstract [5]. Here, the authors employ their custom-built flexible robot [8] to carry a miniature HIFUS probe (ceramic element diameter of 20.15mm). Ex-vivo experiments on chicken breast reveal a manually measured lesion of $6\text{mm} \times 7\text{mm}$ at 3mm below the tissue surface. No further planning and autonomous execution of a more complex ablation field has been explored. Autonomous ablation in the context of brain surgery, including different trajectory planning algorithms was explored in [9], however for a simple planar lab bench setup and abstracted computer vision pipeline.

This work presents the first application of autonomous US-guided HIFUS probe in surgical robotic setting, solving the problem of contact force control and presenting a possible trajectory planning framework, accounting for the tissue surface constraint. As target application this work explore the ablation of liver tumors, where ablation techniques and extracorporeal US imaging are already routinely used.

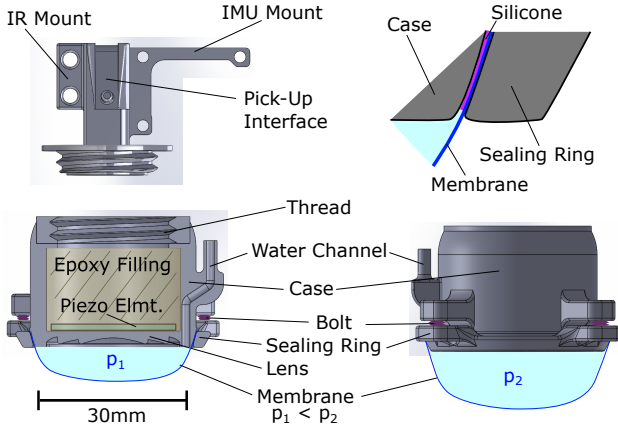


Fig. 2: Cut view of the assembled HIFUS probe design including the epoxy-filled casing with integrated water channels, the sealing ring as well as the piezo element and showing two different inflation states.

II. MATERIALS AND METHODS

A. HIFUS probe design

The main transducer is composed of a cylindrical shell, designed in two parts, which allows the internals to be properly aligned. This includes a piezoelectric disc adhered to an acoustic lens. The void behind the piezoelectric is back filled with a microballoon loaded epoxy as a backing layer. A stiff epoxy was used to fill any tolerance gap surrounding the lens, making the transducer watertight.

A thread at the back allows connecting the transducer with appropriate mechanical interfaces. To interface the probe with a robotic tool, we designed a pick-up interface with a matching thread to fix to the transducer. The pick-up interface is equipped with an Inertial Measurement Unit (IMU) as well as an Infrared (IR) tracking marker for evaluation.

B. Interaction with the Tissue Surface

To solve the issue of acoustic coupling and prevent large reflections at the boundary between tissue surface and transducer, an acoustic impedance matching layer as a water-filled latex membrane was added to the setup that is inspired by [8]. At the same time, being relatively soft, the inflated membrane helps conform to different surface shapes observed on organs in the abdominal cavity.

Considering, the goal of achieving contact control between the relatively soft tissue and the rigid probe it is necessary to measure the contact force or quality to some degree. The goal is to ensure adequate acoustic coupling with the tissue surface while preventing excessive compression. An initial idea was to achieve this by attempting to characterise the change in pressure of the inflated membrane under different loading conditions. This would in theory allow to estimate the contact force between the robotically guided transducer and the tissue surface and ablate the tumor, assuming minimal tissue deformation.

To fit a membrane, we realised a tapered ring design (see Figure 2). The ring is held by four bolts that allow

equal tightening from all side, while reducing buckling. The membrane is spanned in between the ring and the transducer. To ensure water sealing the tapered transducer tip is covered with a thin layer of silicone glue that the ring compresses. To allow feeding water into the membrane to instantiate a static pressure and inflation profile as well as measure the pressure, two 1mm channels were integrated into the casing wall. While a single channel would also allow for pressure measurements, two channels were needed to purge any excess air trapped between the lens and the membrane. This is particularly important to ensure good energy transfer as any trapped air will lead to a strong reflection of the ultrasonic wave back to the transducer. Please refer to Figure 2 for a cut 3D CAD model of the transducer shell.

In addition to the coupling membrane, the probe includes an IMU sensor that is used to perform sensor fusion with robot kinematics for improved accuracy. For that, the sensor fusion scheme from our previous research [10] was adapted and used for both the US probe as well as the HIFUS device.

C. Mechanical Characterisation of the Membrane

To usefully employ the designed membrane in a control context, it became necessary to characterise the material properties of the membrane. An initial analysis revealed that it might be possible to infer the force applied to the tissue surface based on the measured change in pressure change due to compression of the membrane. This measurement in turn allows for control of the forces applied to the tissue surface. A major question was, to what degree the characterisation would change depending on the interactions with surfaces of varying stiffness.

For characterisation, a 3D-printed frame was used to fixate the probe within the experimental setup. To compress the membrane and measure the resulting force the setup employs a manually adjustable linear stage (unknown manufacturer) equipped with a load cell Omegadyne LCM703-10 (Omegadyne Inc., Stamford, CT, USA). The load cell is connected to a HX711 (Avia Semiconductor (Xiamen) Ltd, Xiamen, China) amplifier. The amplifier's analogue output is then transmitted to the Robot Operating System (ROS) network via a Teensy 3.2 (PJRC.COM LLC, Sherwood, OR, USA). The tip of the load cell integrates a 3D printed interface that directly connects to the threaded top of the transducer (see Figure 3).

The characterisation was performed for three different material samples of decreasing stiffness placed under the probe: a rigid surface, a gelatin block, and a chicken thigh. Additionally, experiments were carried out at three different inflation states resulting in varying membrane dome heights (see Figure 2). Initially, the transducer was lowered to the point a which contact was barely made, defined as d_0 (see Figure 3). Subsequently, the transducer was moved down in increments between $25\mu\text{m}$ and $50\mu\text{m}$, depending on the material and the rate of change.

For the pressure-force relationship, a second-order polynomial was found to be the best-fitting model of the lowest complexity. Figure 4 depicts the characterisation results for the pressure/force relationship. Overall, the relationship did not

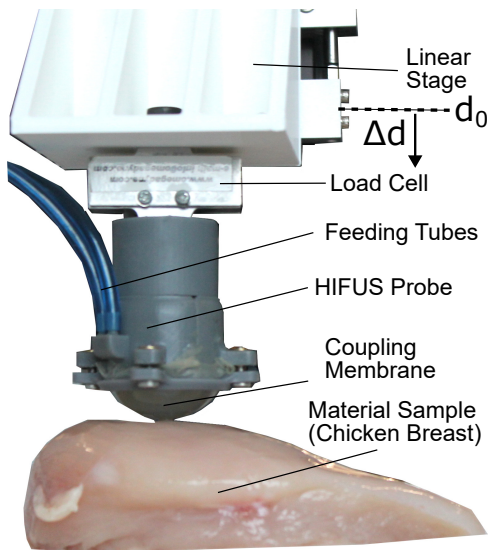


Fig. 3: Test Setup used to characterise the HIFUS membrane. The probe is mounted onto a load cell that attaches to a linearly movable stage.

significantly vary with a change of contact material. While the area over which the pressure is applied does change depending on the material, its variation seems to be low enough to have little effect on the measured force, represented by a low mean Root Mean Square Error (RMSE) of $0.0627N$ over the three fitted curves for different initial pressures. As expected, however, it did vary with initial pressure. For the eventual application during robotic control, the weighted average between the two curves with an initial pressure above and below the current initial pressure was taken. This allowed varying the initial pressure of the system and thereby the compliance as well as the initial dome height of the coupling membrane within the characterised range.

D. Planning and Control Pipeline

The following outlines the planning and pipeline in four steps: (1) surface reconstruction, (2) US scan acquisition, (3) trajectory planning and (4) trajectory execution.

1) *Surface reconstruction:* A crucial initial step is the acquisition of the surface geometry of the organ. For simplicity and repeatability, a gelatine phantom is used with a shape modeled after a typical liver surface. To acquire the surface shape, an Intel RealSense d405 (Intel Corp., Santa Clara, CA, USA) stereo camera is used, with the same working principle as that of a standard endoscopic camera. To enable referencing the point cloud in the local camera frame to the robot, ArUco markers are integrated into a frame with spatial landmarks that allow referencing camera features (ArUco markers) with robotic positions (spatial landmarks). A key challenge with the acquisition of surface data from the gelatine phantom is the lack of features and the high reflectiveness. For this reason, we found the final point cloud to be relatively noisy, resulting in a reduced resolution of only $3mm$ average point distance. Overall, the acquired point cloud resulted in a mean squared error of $0.91mm$. The mean angle error of the normal

vectors calculated from the point cloud was 4.63° and reached a maximum error of 16.95° .

2) *Tumor Scan and Reconstruction:* Based on the surface geometry, the US probe was guided along the surface. The setup used, including the deep learning-based feature detection and contact quality detection, can be found in [10]. To begin with, the probe was placed in the direct vicinity of the mass and displaced in image normal direction towards the mass. Simultaneously, the probe was reoriented to match the surface normal, while maintaining good contact with the tissue surface. Once a tumor feature was identified in the image, the probe was moved along the surface to center that feature in the US frame. After passing over the tumor, the probe was rotated around the tumor by 30 degrees, with the tumor centroid as the pivot point, and scanned again moving over the tumor towards the starting point. This process was repeated a third time, resulting in a total of three scans of the tumor from different angles. We found this process to be more robust against small detection errors, while not causing the robot to run into joint limits e.g. in the case of larger angles than 30 degrees.

3) *Trajectory Planning:* Based on both the acquired surface shape and the reconstructed tumor relating to that surface an ablation path was planned to be followed by the robotically guided HIFUS probe. Planning a trajectory for the laparoscopic HIFUS device is slightly different compared to usual applications in an extracorporeal setting since the target region and probe cannot be immersed in water. Consequently, the planning is highly constrained by the tissue surface, allowing only specific lines of access. To allow proper induction of the ultrasonic waves while preventing collisions between the probe body and the tissue surface, the local surface normals should approximate the direct line of access between the surface point and target location on the tumor. Assuming the surface to be relatively planar (e.g. slightly convex) and thus a relatively constant normal vector within the vicinity of each surface point, this may be approximated by finding the surface points whose connecting vector to the tumor's centroid best approximates the normal vector at that point. This point is identified by iterating through all surface points and checking the angular error between the connecting vector and the surface normal at that point and selecting the one with the lowest deviation between these two vectors.

Once the ideal point is found, the tumor is projected onto the plane with the ideal point's normal vector and located at the centroid. Assuming a relatively convex tumor, the convex hull is then calculated to approximate the outer contour of the tumor projected into that plane. By replicating and scaling down this trajectory a spiraling path is defined that covers the entirety of the tumor similar to the ablation path described in [9]. This process is shown in Figure 6. Lastly, the trajectory is projected onto the surface and each trajectory point is locally shifted in its vicinity ($5mm$ radius) to further improve the matching between the surface normal and the target orientation, representing the connecting vector between the surface point and the target point on the tumor.

4) *Trajectory Execution with Contact Force Control:* To control the probe position, while also integrating the force

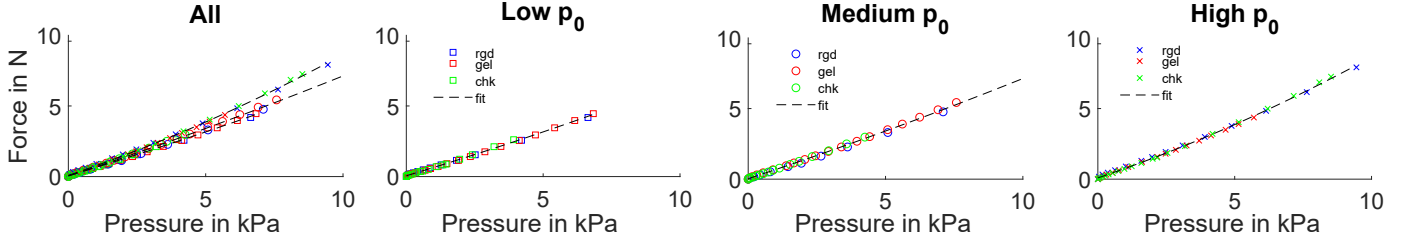


Fig. 4: Membrane Characterisation and subsequent fitting results for membrane pressure (kPa) over force (N) for different materials. Top left shows all data points and fitted curves overlaid, top right, bottom left and bottom right show the data and fitted curves for low, medium and high initial inflation pressure respectively and for different materials.

input from the coupling membrane, a hybrid force position controller was devised [11]. The controller is based in global cartesian space in the following way

$$\begin{aligned} \mathbf{x}_{des,i+1} = & \mathbf{x}_{traj,i+1} + \mathbf{K}_{P,x} \Delta \mathbf{x}_{ctrl,i} + \mathbf{K}_{I,x} \sum_{k=0}^{k=i+1} \Delta \mathbf{x}_{ctrl,i} \\ & + k_{P,f} \Delta \mathbf{f}_{ctrl,i} + k_{I,f} \sum_{k=0}^{k=i+1} \Delta \mathbf{f}_{ctrl,i} \end{aligned} \quad (1)$$

where $\mathbf{x}_{traj,i+1}$ is the pre-calculated position from the trajectory planner at time step $i+1$, $\mathbf{K}_{P,x}$ and $\mathbf{K}_{I,x}$ are diagonal matrices defining the positional proportional and integral gains and $k_{P,f}$ and $k_{I,f}$ are scalar force proportional and integral gains respectively. The positional difference $\Delta \mathbf{x}_{ctrl,i}$ used inside the controller in turn is defined in the following way

$$\Delta \mathbf{x}_{err,i} = \mathbf{x}_{traj,i+1} - \mathbf{x}_{meas,i} \quad (2)$$

$$\Delta \mathbf{x}_{ctrl,i} = \Delta \mathbf{x}_{err,i} - (\Delta \mathbf{x}_{err,i}^T \mathbf{z}_{TT}) \cdot \mathbf{z}_{TT,i} \quad (3)$$

where $\mathbf{x}_{meas,i}$ is the measured position via IMU-fused kinematics at time step i and $\mathbf{z}_{TT,i}$ is the current tool tip z-axis axis (see Figure 1). Equation 3 subtracts the component that is along the tool axis that is determined by the force difference $\Delta \mathbf{f}_{ctrl,i}$ in the following way.

$$\Delta \mathbf{f}_{ctrl,i} = (f_{des} - f_{meas})^T \mathbf{z}_{TT,i} \quad (4)$$

This way it is ensured that the positional control along the tool axis is excluded and fully controlled by the surface normal force. The normal force in turn is extracted from the fitted pressure model. Additionally, the measured pressure is adjusted to account for the hydrostatic pressure. This is achieved by using the robotic end-effector position to calculate the difference in height with respect to the externally fixated pressure sensor.

III. EXPERIMENTAL EVALUATION

The validation experiments for the described approach were carried out in two parts. First, the HIFUS probe was guided along a planar surface in a circular trajectory. This served the purpose of validating the contact force model to control and evaluate the accuracy of a simple trajectory on the surface. In a second study, the system was tested on the gelatine phantom

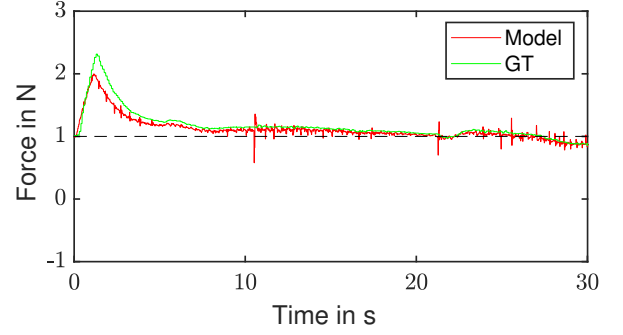


Fig. 5: HIFUS force during execution of planar, circular trajectory.

with an anatomical surface, including the previously outlined planning pipeline to allow conclusions about the application under more realistic circumstances including image guidance. Please note that experiments were carried out with a HIFUS probe dummy that did not deliver ultrasonic energy. The focus here is on evaluating the coupling membrane, planning algorithm and hybrid force-position control. We characterised the device using a hydrophone and assume the dummy probe to exert the measured 3D pressure field.

A. Planar Surface Testing

Three repetitions of circular trajectories on the planar surface with varying diameters ($d = \{10, 20, 30\}mm$) were performed and recorded, giving a total of nine trajectories. In addition to following the trajectory, a target contact force constraint of $1N$ was set.

The results indicate positional errors of $0.6312 \pm 0.3133mm$ between IMU-fused and IR trajectory. The control error, meaning the error between the reference trajectory and IMU-fused kinematics as input into the controller was determined to be $0.8039 \pm 0.3219mm$. Lastly, the error between the IR-tracked, ground truth path and the control input was $1.0212 \pm 0.5021mm$.

Looking at the force control, a slight overshoot at the beginning can be observed that is slowly controlled out throughout the trajectory. Furthermore, a lower peak force is observable, as well as a slight time delay between the measurement with the HIFUS membrane and model and ground truth force measured through the scale. Despite this,

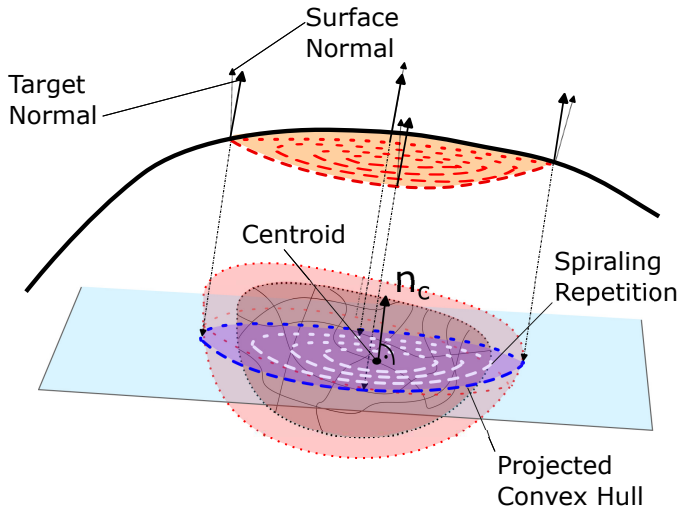


Fig. 6: Depiction of the HIFUS trajectory planning process with n_c the surface normal at the surface point closest to the centroid.

the overall estimation of the model, particularly for static pressure, is as low as $-0.0364 \pm 0.0861N$. Disregarding the first $5s$ in which the controller has not yet reached its steady state, the error is as low as $-0.0135 \pm 0.0448N$. An attempt to increase the P -gain of the controller, leading to a quicker response, led to oscillatory motion of the controller, signaling instability. Eventually, while not ideal, it was decided to leave the controller tuned as shown in Figure 5.

B. Non-Planar Phantom with Ultrasound Guidance

For the non-planar case, the experiments also included three repetitions at three different locations. To validate the system under different tumor locations, the acquired scan was virtually shifted to two other locations, covering different surface topologies while remaining at a similar depth. Subsequently, the reconstructed scans were processed in the trajectory planner. As a starting point, a spiraling trajectory with four concentric circular turns was chosen. An exemplary resulting trajectory is shown in Figure 6. The execution time of these trajectories was around $260s$. As in the prior planar experiments, the desired pressure was set to be $1N$.

Looking at the positional error compared to the planar case, the control error stays roughly similar ($0.96 \pm 0.53mm$) aside from more outliers, the mean error between IMU-fused and IR trajectory was determined at $4.77 \pm 0.91mm$ and at $4.77 \pm 1.03mm$ between IR and control input trajectory. Looking at the force control signal, a good tracking of the constant desired force of $1N$ can be observed (see Figure 8). The mean control error was found to be $0.0088 \pm 0.0689N$.

To get a better idea of the coverage of 3D space by the HIFUS pressure field, the HIFUS pressure field was recorded as a 4D point cloud over time, containing 3D position and pressure intensity. It is assumed that only a pressure over a certain threshold would have a noticeable heating effect on the tissue. Therefore, any points with a pressure intensity lower than 50% of the maximum, equivalent to points outside the

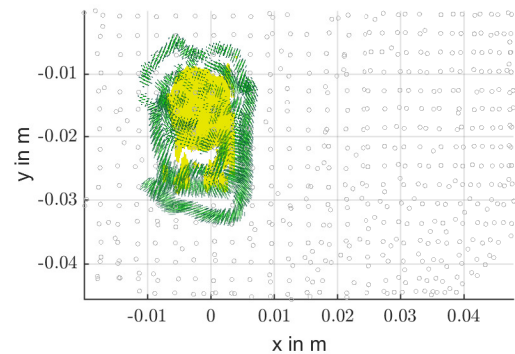
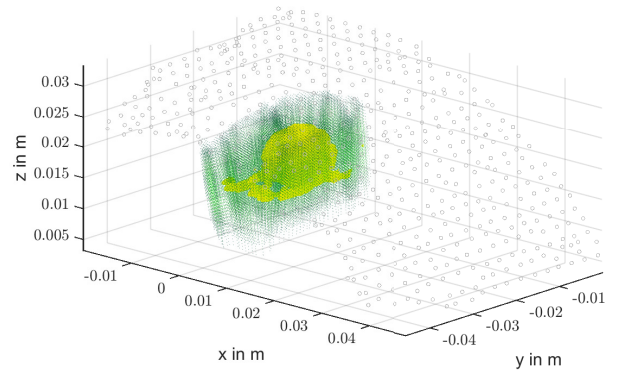


Fig. 7: **Top:** HIFUS tumor coverage in 3D. **Bottom:** HIFUS tumor coverage projection in x-y plane, showing full but coarse coverage of the area.

$-3dB$ line from the Gaussian model, are disregarded. Figure 7 depicts this thresholded pressure point cloud overlaid with the tumor volume. The overlay shows a full coverage of the tumor area with the focal region. As can also be seen on the top view, the trajectories are not nearly dense enough yet, as there are spots that are not fully covered by the HIFUS pressure field point cloud.

Looking at the plot of the trajectories depicted in Figure 1, an offset between the IR-tracked and reference trajectory becomes further apparent. While the IMU-fused trajectory is following the overall shape, the IR-tracked trajectory is offset, despite still resembling a similar shape.

IV. CONCLUSIONS

Comparing the results for the simpler experiment on a planar surface with the more complex scenario of the anatomical surface and target structure, potential sources of the larger error can be identified.

Firstly, as in the previous work presented in this thesis, the applied force has a tremendous effect on the kinematic accuracy of the system. As opposed to the previous applications, US scanning and tissue marking, contact forces between the tool tip and the tissue surface are not supposed to be minimised, but rather enforced to be constant yet very much present. This had a clear effect on the system's accuracy in

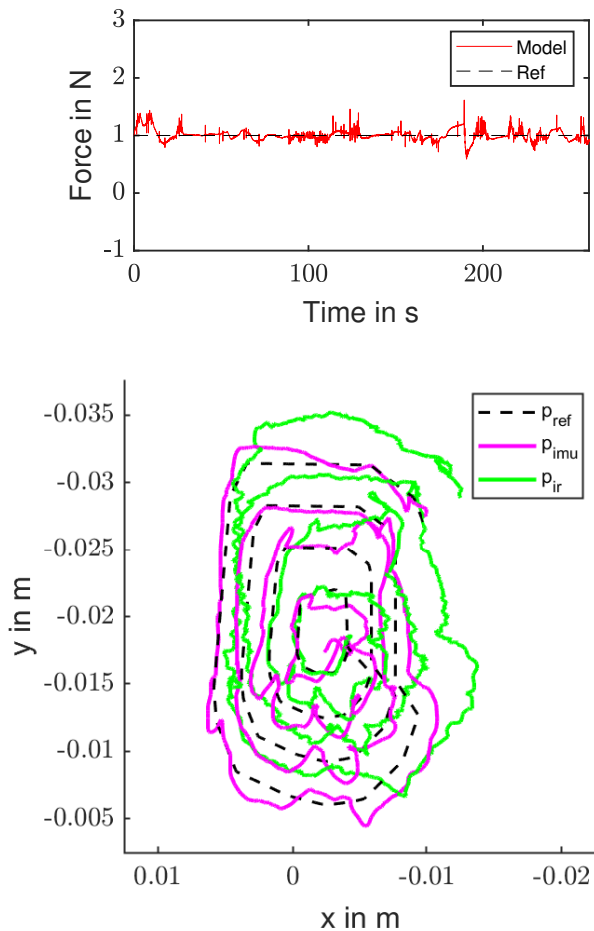


Fig. 8: **Top:** HIFUS forces during execution on non-planar phantom targeting concealed mass. HIFUS tumor coverage in 3D. **Bottom:** HIFUS trajectory as with reference, IMU-fused and IR trajectories.

determining the position despite IMU-fused kinematics. This error is likely very dependent on the exact orientation of the system since different joints are differently accurate and the fusion algorithm does not account for rotations around the gravity axis that are not measured by kinematics itself.

Secondly, the control of the system is performed via a virtually prolonged tool by controlling the positing of the focal point around $25mm$ away from the transducer surface. This means, in consequence, that any orientational error will be further magnified by the longer tool tip resulting in higher positional errors. This becomes especially apparent when comparing the results for the planar execution that had no prolonged tool and did not involve a constantly changing tool orientation.

It remains to be seen how the whole system would perform under induction of real ultrasonic energy into the tissue. Most likely, the robotic execution would need a denser coverage of the surface area, which would in turn mean a longer execution time. As the execution is currently already at over $4min$, this in turn would entail practical considerations as to how long would be acceptable or to what extent the execution time may

be sped up.

When analysing the trajectories, it becomes clear that the grid structure of the surface has a strong effect on how the trajectory is projected upwards. Currently, the surface point cloud is rather coarse at $3mm$ grid size, the resulting trajectories are also relatively edgy. Therefore, a finer grid of the surface would be desirable. For that, a more textured US phantom would need to be created or the system directly evaluated in an ex-vivo setting as done in the previous chapter.

While only accurate within roughly $5mm$, the system still performed well in covering the area around the tumor. In particular, it covered the entire area as previously planned. In the future, it would be desirable to test the system with the application of HIFUS energy and using ex-vivo tissue to explore the real ablation zone. Furthermore, the integration of more models such as the amount of compression of the membrane could allow a more precise control better accounting for tissue deformation.

REFERENCES

- [1] Z. Izadifar, Z. Izadifar, D. Chapman, and P. Babyn, "An introduction to high intensity focused ultrasound: Systematic review on principles, devices, and clinical applications," *Journal of Clinical Medicine*, vol. 9, no. 2, pp. 1–22, 2020.
- [2] A. Cafarelli, M. Mura, A. Diodato, A. Schiappacasse, M. Santoro, G. Ciuti, and A. Menciassi, "A computer-assisted robotic platform for Focused Ultrasound Surgery: Assessment of high intensity focused ultrasound delivery," *Proceedings of the Annual International Conference of the IEEE Engineering in Medicine and Biology Society, EMBS*, pp. 1311–1314, 2015.
- [3] A. Diodato, A. Schiappacasse, A. Cafarelli, S. Tognarelli, G. Ciuti, and A. Menciassi, "Robotic-assisted Platform for USgFUS Treatment of Moving Organs," in *Hamlyn Symposium on Medical Robotics*, pp. 23–24, 2017.
- [4] R. W. Ritchie, T. A. Leslie, G. D. Turner, I. S. Roberts, L. D'Urso, D. Collura, A. Demarchi, G. Muto, and M. E. Sullivan, "Laparoscopic high-intensity focused ultrasound for renal tumors: a proof of concept study," *BJU International*, vol. 107, 2011.
- [5] C. Sozer, A. Cafarelli, M. Brancadoro, and A. Menciassi, "Design and development of a miniaturized intra-abdominal flexible HIFU system: a proof of concept," in *Hamlyn Symposium on Medical robotics*, 2018.
- [6] J. Kim, H. Wu, and X. Jiang, "Miniaturized focused ultrasound transducers for intravascular therapies," in *ASME International Mechanical Engineering Congress and Exposition (IMECE)*, 2017.
- [7] H. Kim, H. Wu, N. Cho, P. Zhong, K. Mahmood, H. Lyerly, and X. Jiang, "Miniaturized Intracavitary Forward-Looking Ultrasound Transducer for Tissue Ablation," *IEEE Trans Biomed Eng*, vol. 67, no. 7, pp. 2084–2093, 2020.
- [8] A. Diodato, M. Brancadoro, G. De Rossi, H. Abidi, D. Dall'Alba, R. Muradore, G. Ciuti, P. Fiorini, A. Menciassi, and M. Cianchetti, "Soft Robotic Manipulator for Improving Dexterity in Minimally Invasive Surgery," *Surgical Innovation*, vol. 25, no. 1, pp. 69–76, 2018.
- [9] Hu, D., Gong, Y., Hannaford, B., and Seibel, E. J., "Semi-autonomous simulated brain tumor ablation with ravenii surgical robot using behavior tree," *2015 IEEE International Conference on Robotics and Automation (ICRA)*. IEEE, 2015.
- [10] Marahrens, N., Scaglioni, B., Jones, D., Prasad, R., Biyani, C.S. and Valdastr, P., "Towards Autonomous Robotic Minimally Invasive Ultrasound Scanning and Vessel Reconstruction on Non-Planar Surfaces," *Frontiers in Robotics and AI*, 9, 2022.
- [11] M. H. Raibert and J. J. Craig, "Hybrid Position/Force Control of Manipulators," *Journal of Dynamic Systems, Measurement, and Control*, vol. 103, pp. 126–133, 06, 1981.